Research Paper

In situ osteoblast mineralization mediates post-injection mechanical properties of osteoconductive material

Callan Bialorucki[a], Gayathri Subramanian[a], Mostafa Elsaadany[a], Eda Yildirim-Ayan[a,b,*]

[a]Department of Bioengineering, College of Engineering, University of Toledo, Toledo, OH 43606, USA
[b]Department of Orthopaedic Surgery, University of Toledo Medical Center, Toledo, OH 43614, USA

ARTICLE INFO

ABSTRACT

The objective of this study was to understand the temporal relationship between *in situ* generated calcium content (mineralization) and the mechanical properties of an injectable orthobiologic bone-filler material. Murine derived osteoblast progenitor cells were differentiated using osteogenic factors and encapsulated within an injectable polycaprolactone nanofiber-collagen composite scaffold (PN-COL +*osteo*) to evaluate the effect of mineralization on the mechanical properties of the PN-COL scaffold. A comprehensive study was conducted using both an experimental and a predictive analytical mechanical analysis for mechanical property assessment as well as an extensive *in vitro* biological analysis for *in situ* mineralization. Cell proliferation was evaluated using a PicoGreen dsDNA quantification assay and *in situ* mineralization was analyzed using both an alkaline phosphatase (ALP) assay and an Alizarin Red stain-based assay. Mineralized matrix formation was further evaluated using energy dispersive x-ray spectroscopy (EDS) and visualized using SEM and histological analyses. Compressive mechanical properties of the PN-COL scaffolds were determined using a confined compression stress-relaxation protocol and the obtained data was fit to the standard linear solid viscoelastic material mathematical model to demonstrate a relationship between increased *in situ* mineralization and the mechanical properties of the PN-COL scaffold. Cell proliferation was constant over the 21 day period. ALP activity and calcium concentration significantly increased at day 14 and 21 as compared to PN-COL −*osteo* with undifferentiated osteoblast progenitor cells. Furthermore, at day 21 EDS, SEM and von Kossa histological staining confirmed mineralized matrix formation within the PN-COL scaffolds. After 21 days, compressive modulus, peak stress, and equilibrium stress demonstrate significant increases of 3.4-fold, 3.3-fold, and 4.0-fold respectively due to *in situ* mineralization. Viscoelastic parameters calculated through the standard linear solid mathematical model fit to the stress-relaxation data

---

*Corresponding author at: Department of Bioengineering, College of Engineering, University of Toledo, Toledo, OH 43606, USA. Tel.: +1 419 530 8257; fax: +1 419 530 8030.
E-mail address: eda.yildirimayan@utoledo.edu (E. Yildirim-Ayan).

also indicate improved mechanical properties after *in situ* mineralization. This investigation clearly demonstrates that *in situ* mineralization can increase the mechanical properties of an injectable orthobiologic scaffold and can possibly guide the design of an effective osteoconductive injectable material.

1.   Introduction

Current treatment techniques for irregular shaped bone fractures involve the injection of bio-inert bone filler materials such as polymethylmethacrylate (PMMA) or bioactive resin-based materials such as calcium phosphate cement (CaP) (Blattert et al., 2009; Welch et al., 2002; Tarsuslugil et al., 2013; Heo et al., 2009; Grafe et al., 2008; Galovich et al., 2011; Arabmotlagh et al., 2012) to the defect area via minimally invasive techniques. These widely accepted, time-honored techniques provide rapid pain relief and allow for instant primary stability of the fracture site due to the rapid polymerization of the injected material. However, both PMMA and calcium content resin-based materials fall short of clinical expectations in several ways including their exothermic polymerization process, a lack of regenerative potential and significant mismatch in mechanical properties as compared to native bone (Blattert et al., 2009; Welch et al., 2002; Tarsuslugil et al., 2013; Heo et al., 2009; Grafe et al., 2008; Galovich et al., 2011; Arabmotlagh et al., 2012). PMMA's highly exothermic polymerization and cytotoxic monomer composition can also lead to adjacent tissue necrosis (Blattert et al., 2009; Tarsuslugil et al., 2013; Heo et al., 2009). The lack of participation in bone remodeling and the significant mismatch in mechanical properties between bioinert filler materials and native bone can lead to stress shielding and adjacent bone resorption around the host fractured area (Welch et al., 2002; Heo et al., 2009; Galovich et al., 2011; Arabmotlagh et al., 2012). Taking into consideration the clinical drawbacks of current injectable bone filler materials, there is a demand for a new generation injectable, orthobiologic material with an ability to stabilize a fracture site and to provide an environment for bone regeneration and remodeling.

Efforts have been made toward developing a variety of injectable cell-encapsulated hydrogels (Chen et al., 2012; Huang et al., 2011, 2009; Niranjan et al., 2013; Xia et al., 2012) as well as hydrogel-polymeric microsphere injectable biomaterials (Shen et al., 2010, 2013; Yang et al., 2010) for bone tissue regeneration. For instance, Ding et al. (2013) demonstrated the potential of injectable chitosan/β-glycerophosphate/collagen scaffold in terms of its biocompatibility, osteogenic potential, and bone regeneration with both *in vitro* and *in vivo* studies. Niranjan et al. (2013) demonstrated the potential of a zinc-chitosan-β-glycerophosphate thermosensitive injectable hydrogel composite as a scaffold for bone tissue regeneration. Shen et al. (2010) studied *in situ* polymerizable and injectable rhBMP-2-loaded/PLGA/hydroxyapatite microspheres on osteoblast differentiation and proliferation. Our group also developed an *injectable* nanofibrous scaffold called PN-COL composed of polycaprolactone (PCL) nanofibers interspersed within a collagen Type-I solution to address the need for an injectable, osteoconductive material for bone regeneration. In a previous study, PN-COL was successful in maintaining cell viability and demonstrating osteoblast late stage differentiation Baylan et al. (2013).

These injectable scaffolds provide an opportunity to introduce cells and other biological cues to a defect site to promote bone regeneration. However, appropriate mechanical cues are also necessary for successful bone regeneration which requires scaffolds to have appropriate mechanical properties (Deng et al., 2011). The majority of bioactive injectable scaffolds have suffered from poor mechanical properties due to the innate gel-like structure necessary for injectability. Their gel-like structure, which allows for cell/protein accommodation within these scaffolds, hinders their mechanical performance for serving as bone tissue scaffolds. From *in vivo* and clinical studies, it is known that there is a positive correlation between mineral content and mechanical properties of bone (Currey, 1969, 1975, 1988, 2001; Roy et al., 2001). Studies have also shown that synthetic mineralization through the incorporation of minerals such as hydroxyapatite (HA) to the scaffold and cell-induced mineralization of collagen scaffolds have increased scaffold mechanical properties (Deng et al., 2011; Heinemann et al., 2011; Khanarian et al., 2012; Li et al., 2013; Liao et al., 2011; Marelli et al., 2011; Meng et al., 2007; Wahl and Czernuszka, 2006).

Taking into consideration the biological phenomena presented in the literature, it is expected that the PN-COL scaffold will incur similar increases in mechanical properties. Therefore, the objective of this study was to understand the temporal relationship between *in situ* generated calcium content (mineralization) and the mechanical properties of the injectable PN-COL scaffold. In order to accomplish this objective, PN-COL scaffolds were cultured with osteoblast cells and cell-induced mineralization was tracked over 21 days along with the changes in mechanical properties. A confined compression stress-relaxation protocol and the standard linear solid model were used in this study to measure the changes in the viscoelastic compressive mechanical properties of PN-COL over time. Cell proliferation and mineralization assessments including DNA quantification, alkaline phosphatase (ALP) activities, and mineral content quantification were run to characterize mineralization over time. Furthermore, calcium and phosphorous content was verified within the scaffold using energy dispersive x-ray spectroscopy (EDS) and mineralized matrix formation was visualized using SEM and histological analyses. This study can possibly guide the design of an effective osteoconductive injectable material through considering the effect of cells'

presence on the structural integrity of injectable bone tissue scaffolds.

2. Methods and materials

2.1. Fabrication of the injectable scaffold

The composite, injectable polycaprolactone-collagen (PN-COL) biomaterial was obtained by incorporating electrospun poly-caprolactone (PCL) nanofibers within collagen Type-I solution. PCL (M_w=45,000, Sigma-Aldrich) nanofibers were obtained via an electrospining technique. A 16% (w/v) PCL solution was prepared by dissolving PCL in a 3:1 chloroform/methanol (v/v) solution and delivering the solution through a syringe with a 20-gauge needle connected to a syringe pump (New Era Pump Systems, Inc.). The solution was fed with a rate of 8000 μl/h to the electrical field created by applying 20 kV to the needle using a high voltage power supply (ES30P, Gamma High Voltage) and grounding the collection plate. The electrospinning process was carried out under ambient conditions of $25\pm3\,°C$ temperature with $50\pm5\%$ relative humidity for 45 min. The fibrous meshes on the collection plate were peeled and dried in a desiccator for 72 h to remove residual organic solvent and moisture. The PCL nanofiber mats were then homogenized using a high-speed homogenizer (Ultra-Turrax, IKA Works, Inc). Prior to mixing the PCL nanofibers with collagen Type-I solution, PCL nanofibers were functionalized with oxygen-based plasma for 3-min to introduce oxygen-containing functional groups on the nanofibers and to reduce the hydrophobicity of the nanofibers (Yildirim et al., 2011).

The functionalized PCL nanofibers were mixed with neutralized collagen Type-I solution (BD Biosciences, USA). The purchased collagen Type-I solution had a concentration of 3.41 mg/ml with a pH of ~3–4. This collagen solution was diluted to 2.5 mg/ml and the pH was neutralized to 7.0 with chilled 1 M sodium hydroxide, PBS, and deionized water in order to induce collagen polymerization. The plasma-treated PCL nanofibers were then mixed with the prepared collagen solution in a ratio of 6% (w/v) to obtain the injectable composite PN-COL scaffold prior to cell encapsulation.

PN-COL cell-encapsulated scaffolds were prepared in 48-well plates for cellular characterization and mechanical testing. Prior to encapsulation within the PCL-Collagen Type I solution, pre-osteoblast MC3T3-E1 (ATCC, CRL-2593; USA) cells were cultured for 3 days in a complete media of α-minimum essential medium (α-MEM) (Life Technologies; USA) supplemented with 1% antibiotics (Life Technologies; USA), 10% fetal bovine serum (FBS) (Gibco; USA), and osteogenic factors including 10 mM β-glycerophosphate and 50 μg ml^{-1} ascorbic acid. For the remainder of this manuscript, this sample group will be referred to as "PN-COL +osteo". Control samples (PN-COL −osteo) were prepared by encapsulating pre-osteoblast MC3T3-E1 (ATCC, CRL-2593; USA) cells cultured in the same media without osteogenic factors. All scaffolds were prepared with a cell density of 10^6 cells ml^{-1} and were allowed to polymerize in 48-well plates at 37 °C and 5% CO_2. Both PN-COL +osteo and PN-COL −osteo scaffolds were cultured in each respective media until the characterization day.

2.2. Assessing cell viability and mineralization capacity of the injectable scaffold

2.2.1. Cell proliferation

Cell proliferation within the PN-COL scaffold was assessed using a fluorescent PicoGreen dsDNA quantification assay (Life Technologies; USA). Briefly, the scaffold samples were snap frozen in liquid nitrogen and crushed to liberate the cells within the scaffold. A DNA lysis buffer (50 mM Tris HCl, 1 mM $CaCl_2$, pH=8) along with proteinase K in a 200 μg/ml concentration was added to the scaffolds and the mixture was incubated overnight at 50 °C. After incubation, the samples were centrifuged and the supernatant was removed. Per manufacturer protocol, the samples were then diluted 1:10 in TE buffer, the PicoGreen dye was diluted 1:200 in $1\times$ TE buffer and the two solutions were mixed in a 96-well plate in a 1:1 ratio. The PicoGreen dye was protected from light throughout the duration of the protocol as it is susceptible to photodegradation. Two minutes after mixing the DNA sample with the diluted dye, the samples were read in a fluorometer at 480 nm excitation, 520 nm emission. Total DNA was determined from the fluorescence reading using a standard curve generated using a serial dilution of stock dsDNA.

2.2.2. Alkaline phosphatase activity

The alkaline phosphatase (ALP) activity of the PN-COL scaffolds was evaluated using alkaline phosphatase colorimetric assay (Sigma-Aldrich, USA) at Day 7, 14, and 21 (n=4). The assay measures p-nitrophenol (pNP) converted from p-nitrophenyl phosphate (pNPP) in the presence of ALP. The rate of pNP production is linearly proportional to ALP activity. Prior to ALP analysis, the scaffolds were washed to remove all media from within the scaffold. The encapsulated cells were liberated by snap freezing the scaffolds in liquid nitrogen and crushing the frozen scaffolds. An alkaline lysis buffer (10 mM Tris–HCl, 2 mM $MgCl_2$, 0.1% Triton X-100, pH 8) was added to the crushed scaffold and the solution was homogenized using high-speed homogenizer. The samples were centrifuged and the supernatant was collected for assaying. The pNPP substrate was then added in a 1:1 ratio to the supernatant in a 96-well plate and the solutions were incubated for 30 min at 37 °C. A 3 N NaOH stop solution was used and the pNP production was determined by measuring the absorbance at 405 nm using a microplate reader (SOFTmax Pro). To convert the measured absorbance to a pNP value, a standard curve was established using a serial dilution of the ALP enzyme. Results were normalized with respect to total cell protein levels calculated by following the manufacturer's protocol for a standard Bradford assay, Coomassie Plus (Bradford) Assay Kit (Thermo Scientific, USA). Briefly, the cell lysate was mixed with the Coomassie Plus™ Reagent and incubated for 10 min at room temperature. Absorbance was measured at 595 nm and total protein was determined using a standard curve of known BSA concentrations.

2.2.3. Matrix mineralization

The progression of calcium deposition due to matrix mineralization within/on the PN-COL composite scaffolds was quantified using an Alizarin Red stain-based assay (Millipore, catalog # ECM815; USA). Constructs containing cells were snap frozen in

liquid nitrogen and crushed to expose all calcium deposits. The scaffolds were then incubated for 20 min in Alizarin Red stain to allow sufficient time for the stain to bind with mineralized calcium. Following the incubation, a series of PBS washes were conducted to remove all excess Alizarin Red stain. The samples were then incubated in 10% acetic acid for 30 min, centrifuged and the supernatant was removed for boiling. The samples were then boiled at 85 °C for 10 min and followed by 5-minute incubation on ice. The samples were then neutralized (pH range 4–4.5) by adding of 10% NH_4OH and centrifuged for 10 min at 14000 rpm. The supernatant was then added to 96-well plate to be read by microplate reader (SOFTmax Pro) at an absorbance of 405 nm. A standard curve was generated to correlate the 405 nm absorbance reading to Alizarin Red concentration. Results were normalized with respect to total cell protein levels calculated by following the manufacturer's protocol for a standard Bradford assay, Coomassie Plus (Bradford) Assay Kit (Thermo Scientific, USA). Briefly, the cell lysate was mixed with the Coomassie Plus™ Reagent and incubated for 10 min at room temperature. Absorbance was measured at 595 nm and total protein was determined using a standard curve of known BSA concentrations.

2.2.4. Morphology and mineral mapping

The morphological and mineral content changes due to *in situ* mineralization were examined using Scanning Electron Microscopy (SEM) (Quanta 3D FEG). Prior to SEM analysis, PN-COL scaffolds were fixed with 4% paraformaldehyde solution (Sigma) for 1 h and then post-fixed in 1% (v/v) osmium tetroxide diluted with Sorensen's buffer to enhance the image quality. After fixation, the samples were dehydrated first in sequential ethanol solutions with increasing concentrations from 30% to 100%. Dehydration was then continued by submerging samples into sequential ethanol/hexamethyldisilazane (HMDS) solutions from 30% to 100% for 15-min each. The samples were air-dried under a chemical hood over-night to evaporate the residual ethanol and HMDS. The dried samples were then gold sputter coated for visualization and mineral content measurement through energy-dispersive x-ray spectroscopy (EDS).

2.2.5. Histology analysis

The mineralization content and cells within the injectable matrix were visualized using a histological analysis and von Kossa staining. On characterization day (day 7, 14, and 21), the PN-COL scaffolds were removed from incubator and were incubated in 10% formalin overnight, dehydrated using an ethanol gradient, and then cleared with xylene before embedding them in paraffin. The paraffin-embedded samples were sectioned at 20 µm thickness using a microtome and mounted on microscope slides. A von Kossa stain was utilized to visualize mineralization within the PN-COL scaffold.

2.3. Assessing and predicting mechanical properties of the injectable scaffold

2.3.1. Mechanical testing

To characterize the time-dependent viscoelastic behavior and the compressive modulus of the PN-COL scaffolds, a confined compression ramp stress-relaxation protocol was employed. All mechanical testing was conducted at room temperature using a bench top mechanical testing device (Electroforce 3200, Bose; USA) with a 1000 g (10 N) load cell. A custom made confined compression fixture was designed to eliminate lateral expansion of the cultured samples by mimicking the dimensions of the 48-well plate used to culture the scaffolds (Fig. 1). The confining chamber allowed for 0.15 mm clearance between the well and the 40 µm stainless steel, porous filter. Cylindrical samples ($n=6$) were removed from the culture condition, sample height was measured using digital calipers, and then each sample was placed in the custom-made confined compression fixture. The samples were equilibrated to a tare load of 0.1 g (0.001 N) to ensure circumferential contact with the cylindrical PN-COL sample. Following the tare loading cycle, one linear ramp compression displacement was applied to the sample at a strain rate of 1%/s until 20% strain, followed by a constant displacement for 300 s. A stress-strain profile (σ vs. ε) and stress-time profile (σ vs. t) were generated using the data collected from the stress-relaxation protocol and the peak stress, equilibrium stress, and compressive modulus of the PN-COL sample were calculated. The compressive modulus of each sample was determined as the slope of the linear stress-strain profile between 0 and 20% strain. Equilibrium stress was calculated as the average stress of the final 100 s in the relaxation phase.

2.3.2. Predictive viscoelastic mathematical model

Various mathematical models have been developed to describe the non-linear viscoelastic behavior of materials such as creep, stress-relaxation, and recovery (Wang et al., 2013). In this study, the Standard Linear Solid (SLS) model was adopted because this model has been shown to precisely simulate the behavior of a wide range of viscoelastic materials (Trickey et al., 2000; Shazly et al., 2008).

This SLS model was utilized to predict the time-dependent stress and the material viscoelastic behavior of the PN-COL +*osteo* as dictated by Eq. (1).

$$\sigma(t) = \varepsilon_0[K_e + K_1^* \exp(-t/\tau)] \tag{1}$$

where ε_0 is the strain applied to the viscoelastic material during the stress-relaxation test; K_e and K_1 are the elastic moduli of the associated spring; t is the time; and τ is relaxation time which is also defined as the ratio of material's viscosity (η) to elastic modulus of spring constant K_e. The stress-time curve obtained from SLS model and experimental data were compared to predict the elastic modulus and viscosity of the PN-COL scaffold.

2.4. Statistical analysis

Statistical analysis was performed using a One-Way ANOVA with a minimum confidence level of 0.05 for statistical significance and a post-hoc Tukey HSD. All values are reported as the mean and standard deviation of the mean.
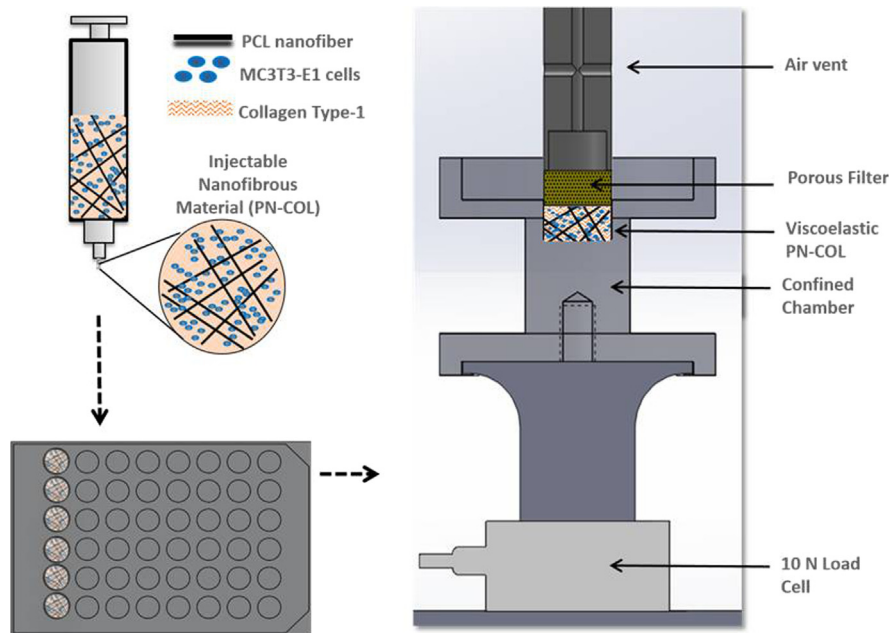
Fig. 1 – Schematic of the mechanical testing set-up. The injectable scaffold was polymerized and cultured in 48-well plates before being transferred to the confined chamber. The confining fixture was attached to a 1000 g (10 N) load cell of the Bose Electroforce 3200 mechanical testing device and the samples were subjected to a ramp displacement stress-relaxation protocol. The indenter of the apparatus performed the compression of the scaffold. The indenter included an adhered 40 micron porous filter and a vent to prevent vacuum formation upon compression of the viscoelastic PN-COL sample.

3. Results

3.1. Cell viability and mineralization

3.1.1. DNA quantification

Cell proliferation was characterized using a PicoGreen dsDNA quantification assay ($n=4$) at day 7, 14, and 21 (Fig. 2). PN-COL $-osteo$ and PN-COL $+osteo$ samples were seeded with a cell density of 10^6 cells ml^{-1} (400,000 cells). Both PN-COL $-osteo$ and PN-COL $+osteo$ samples maintain a DNA count of around 2500 ng over 21 days. The constant DNA count suggests that the PN-COL scaffold did not induce proliferation but instead supported a maintained cell number over the 21 day culture period.

3.1.2. Alkaline phosphatase activity

Alkaline phosphatase is a known osteoblastic differentiation marker. Therefore, a quantitative analysis of alkaline phosphatase activity will demonstrate the initialization of matrix mineralization for the cells within the PN-COL scaffold. Fig. 3A shows the alkaline phosphatase activity normalized against total protein content for both control and experimental groups. As expected, control samples demonstrated very little ALP activity throughout the first 14 days of cultivation. At day 21, the control sample indicates a significant increase in alkaline phosphatase activity. After 14 and 21 days of culture, experimental samples demonstrate a significant increase in alkaline phosphatase activity suggesting the onset and continuation of osteoblast matrix mineralization.
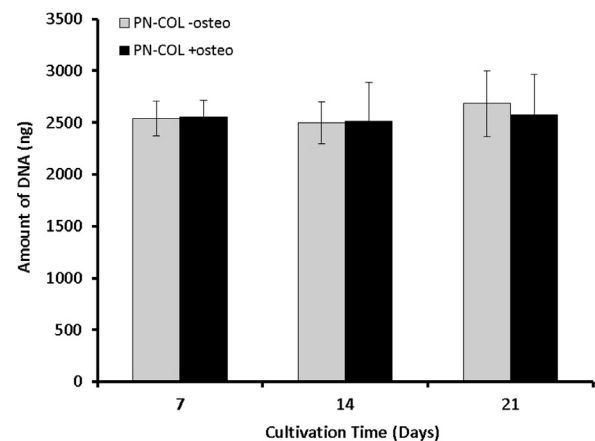

Fig. 2 – DNA quantification ($n=4$) of PN-COL $-osteo$ and PN-COL $+osteo$ scaffolds at day 7, 14, and 21. DNA content in all scaffolds remained relatively constant over the 21-day cultivation period with no significant differences between PN-COL $-osteo$ and PN-COL $+osteo$ scaffolds.

3.1.3. Matrix mineralization

Mineralized matrix was confirmed at day 14 and 21 using an Alizarin Red stain-based assay. Fig. 3B shows the calcium deposition concentration normalized against total protein content for both control and experimental groups. At day 14 and 21, the experimental group demonstrated a significant increase in calcium deposition concentration indicating a significant increase in encapsulated osteoblast mineralization. These results are consistent with the alkaline phosphatase data.
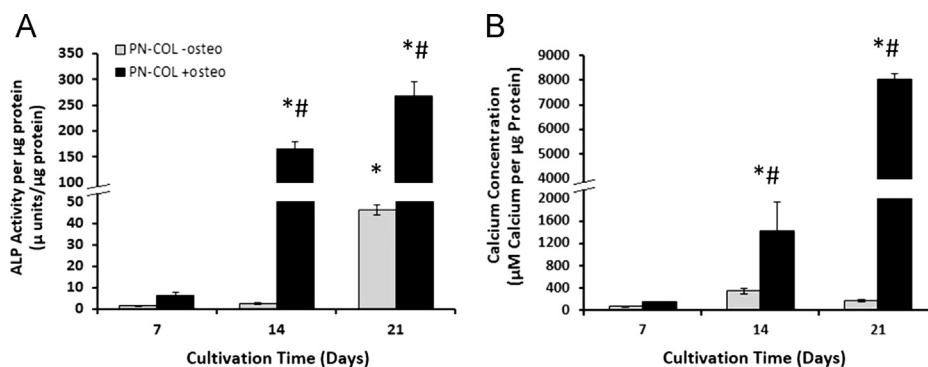
Fig. 3 – (A) Alkaline phosphatase activity and (B) calcium concentration normalized against total protein of PN-COL −osteo and PN-COL +osteo (n=4) within the PN-COL scaffold from Day 7 to Day 21. Both ALP activity and calcium concentration demonstrate significant increases at day 14 and 21. (*) indicates significant difference as compared to earlier time points of the same sample group. (#) indicates significant difference as compared to same day PN-COL −osteo (control) $p < 0.05$.

3.1.4. Morphology and mineral mapping

After 21 days of culture, both PN-COL −osteo and PN-COL +osteo samples were visualized using scanning electron microscopy. The white and solid crystalline structures on the PN-COL +osteo scaffolds were mineralized crystals deposited by the encapsulated cells (Fig. 4B). As demonstrated in Fig. 4A and B, PN-COL +osteo samples contained numerous mineralized deposits, whereas mineral deposits were absent for the control sample (PN-COL −osteo). Furthermore, energy dispersive x-ray spectroscopy was utilized to identify mineral content within both samples at the day 21 mark as well. Fig. 4 shows noticeable increases in both calcium (C, D) and phosphorus (E, F) within the PN-COL +osteo samples as compared to the control (PN-COL −osteo). The EDS spectrum (Fig. 4G and H) reveals a noticeable peak at 3.69 keV indicative of a composition containing calcium for the PN-COL +osteo sample at day 21 which is absent in the PN-COL −osteo control.

3.1.5. Histology analysis

Further visualization of mineralized matrix deposition within the PN-COL +osteo samples was demonstrated using a histological analysis and a von Kossa stain (Fig. 5). Histological examination with von Kossa staining of PN-COL +osteo revealed no mineralized matrix at day 7 and a slight indication of mineralized matrix deposition at day 14. However, at day 21 von Kossa staining reveals an apparent increase in mineralized matrix, which is consistent with the previous mineralized matrix characterizations within this study.

3.2. Compressive mechanical characterization

3.2.1. Confined compression stress-relaxation

Confined compression testing of experimental and control PN-COL −osteo samples provided stress responses with well-defined ramp, peak, and relaxation phases (Fig. 6A). The mineralized PN-COL samples demonstrate a typical viscoelastic response with a significant increase ($p < 0.05$) in peak and equilibrium stresses after 21 days of culture. The average equilibrium and peak stresses for each time point are displayed in Fig. 6B and C. After 21 days of culture, the PN-COL +osteo samples demonstrated a significant increase ($p < 0.05$)

in equilibrium stress and peak stress whereas the undifferentiated samples did not demonstrate any significant difference. The compressive modulus for each sample is displayed in Fig. 6D. PN-COL +osteo samples also demonstrate a significant increase ($p < 0.05$) at day 14 and 21 as compared to PN-COL −osteo (control) and day 0 samples. After 21 days of culture, the compressive modulus of the PN-COL +osteo samples increased 3.4 fold from 1.64 ± 0.37 kPa at day 0 to 5.62 ± 1.39 kPa at day 21. Similar increases can be seen in equilibrium and peak stresses.

3.2.2. Mechanical properties and mineralization correlation

The correlation between calcium concentration and compressive modulus is illustrated in Fig. 7A. Significant increases in compressive modulus and calcium concentration at day 14 and 21 contribute to the increasingly positive linear correlation seen in Fig. 7A.

3.2.3. Predictive viscoelastic behavior

A non-linear regression was performed using MathCAD software to fit the equation of the standard linear solid (SLS) model (Eq. (1)) to the averaged experimental stress-relaxation data generated for PN-COL +osteo on day 0, 7, 14, and 21. A graph representing the stress-time profiles of SLS model and experimental data at all-time points is given in Fig. 7B.

The stress-time profile obtained from the SLS model demonstrated great agreement with stress-time data from the stress-relaxation evaluation of PN-COL +osteo all time points (Fig. 7B). The coefficient of determination (R^2) ranged from 0.942 to 0.970 between the mathematical model and the experimental data indicating the standard linear solid model was appropriate for predicting the viscoelastic parameters of the PN-COL material. The viscoelastic parameters (τ, η, K_e and K_1) of the mineralized PN-COL material were calculated using a non-linear regression analysis (Table 1). At day 21, the PN-COL +osteo samples demonstrate an apparent increase in viscosity (η), and elastic moduli (K_e and K_1) as compared to those at day 0, 7, and 14.
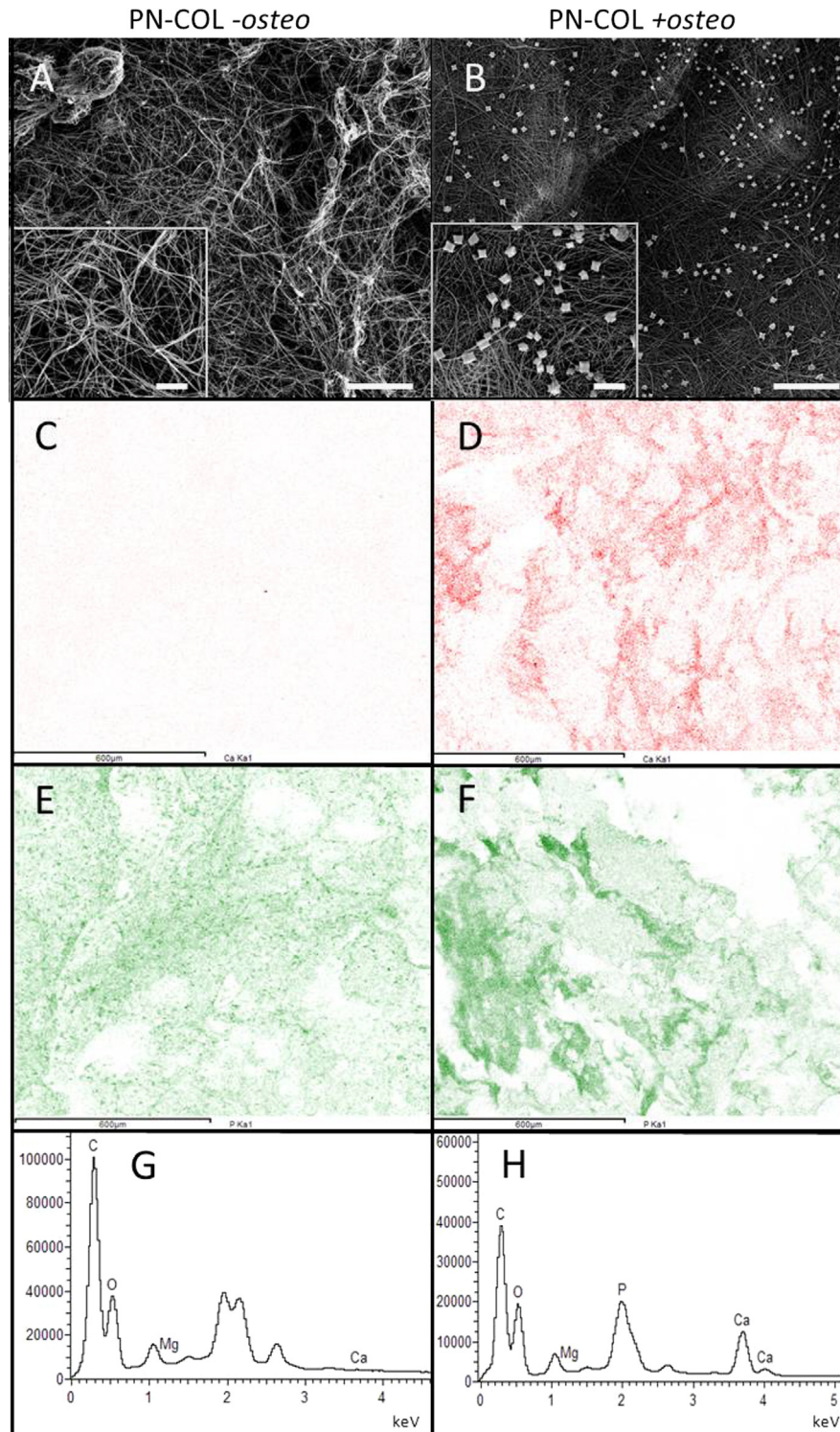
PN-COL *-osteo*   PN-COL *+osteo*

Fig. 4 – SEM micrographs (A) and (B), EDS distribution maps of calcium (C) and (D) and phosphate (E) and (F) minerals, and EDS spectral analysis of PN-COL scaffolds (G) and (H) after 21 days of culture. Scale bars of SEM micrographs represent 20 μm and 5 μm respectively.

4.   Discussion

Injection of bioinert PMMA (bone cement) and calcium content resin materials such as CaP are considered gold-standards for stabilizing irregular-shape bone fractures due to their inherent mechanical strength and rapid polymerization. For clinical applications, healing and regeneration capacity of bone filler materials are as important as strength and stability. Cell/protein-loaded, injectable orthobiologic materials have the potential to be great alternatives to the currently
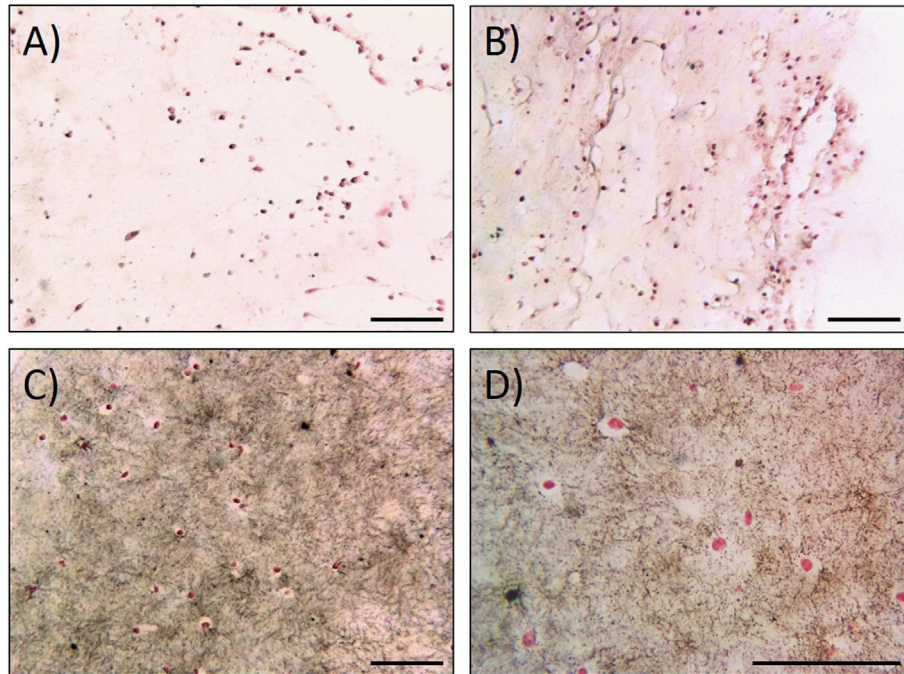
Fig. 5 – Histology slices of PN-COL +*osteo* **after 7 days (A), 14 days (B), and 21 days (C) and (D) of culture. Von Kossa staining reveals the progression of mineralized matrix secretion within the PN-COL** +*osteo* **samples. Pink dots represent the nucleus of cells within the matrix. Brown dots represent the mineralized matrix. Scale bar represents 100 μm.**
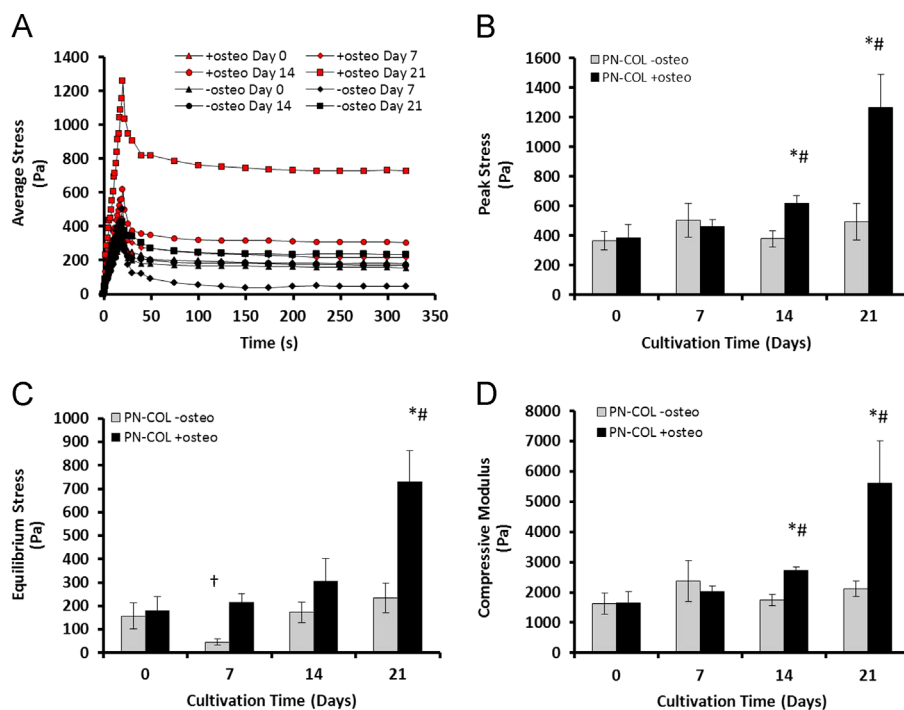

Fig. 6 – (A) Average compressive stress of PN-COL +*osteo* **($n=6$) in response to confined compression stress-relaxation (strain rate $=1\%$/sec). (B) Average peak stress, (C) average equilibrium stress and (D) compressive modulus of PN-COL samples over 21 days of culture ($n=6$). Error bars represent one standard deviation with (*) representing significant difference as compared to earlier time points of the same sample group and (#) representing significant difference as compared to same day PN-COL** −*osteo* **(control) with $p<0.05$. (†) Day 7 of PN-COL** −*osteo* **indicated a significantly decreased ($p<0.05$) equilibrium stress as compared to all other control samples.**
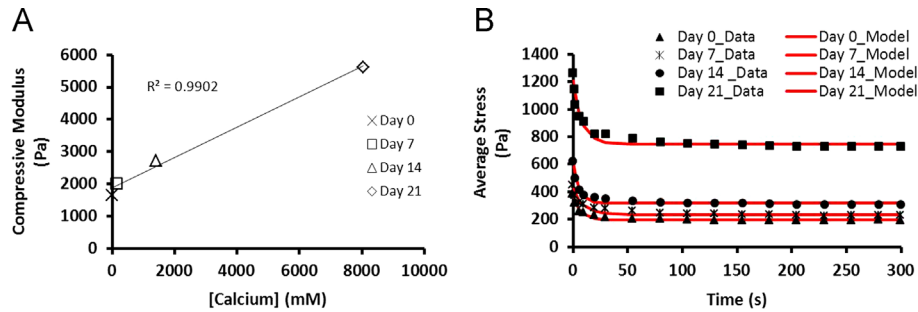
A

B

Fig. 7 – (A) Compressive modulus as a function of calcium concentration. Represented here is the increasingly positive linear relationship between calcium deposition and compressive modulus of the PN-COL material. (B) Standard Linear Solid model curve fitting for averaged confined compression stress-relaxation data for day 0–21 samples of PN-COL +osteo.

Table 1 – Viscoelastic parameters of mineralized PN-COL +osteo at Day 0–21.

Day	K_e (Pa)	K_1 (Pa)	η (Pa s)	τ (s)	R^2
0	968.62	877.36	6,949	7.174	0.967
7	1174	939.1	1,1396	9.707	0.942
14	1593	1441	9,018	5.661	0.97
21	3743	2290	30,527	8.156	0.949

used bioinert injectable materials; however, injectable ortho-biologic materials have poor mechanical properties inherent in their injectable viscoelastic nature. We hypothesized that in situ mineralization within the injectable orthobiologic PN-COL scaffold can mediate its mechanical properties over cultivation time. The objective of this study was to understand the temporal relationship between in situ generated calcium content (mineralization) and the mechanical properties of the injectable scaffold. We have used a novel injectable scaffold, PN-COL, with encapsulated pre-osteoblast cells as an injectable bone-filler material. Two experimental groups were used to assess the effect of mineralization on the mechanical properties of PN-COL. The first group was the PN-COL −osteo group cultured without osteogenic factors, which served as a control group. The second group was the PN-COL +osteo group cultured with the osteogenic α-MEM to induce mineralization. A comprehensive study was conducted using both an experimental and a predictive mathematical model for the assessment of mechanical properties and an extensive in vitro biological analyses for in situ mineralization.

A 21-day in vitro study was conducted to demonstrate that the PN-COL material is able to accommodate pre-osteoblast cells and to allow mineralized matrix accumulation within its structure. DNA content was quantified at day 7, 14, and 21 and it was demonstrated that cells encapsulated within the injectable scaffold maintained a constant cell number throughout the 21 days of culture. Alkaline phosphatase (ALP) activity and calcium deposition were quantified at day 7, 14, and 21. ALP activity, an early osteogenic differentiation marker, significantly ($p<0.05$) increased in PN-COL +osteo samples at day 14 and 21 indicating the onset and continuation of osteoblast mineralization (Fig. 3A). The mineralization data measured using an alizarin red stain-based assay demonstrated a significant ($p<0.05$) increase in calcium deposition within the

PN-COL +osteo group at day 14 and 21 as compared to its counterparts in the control PN-COL −osteo group (Fig. 3B). Looking at the trend of ALP and calcium concentration data, it becomes apparent that, if the study were to be carried out to 28 days, it is likely that the PN-COL +osteo samples will continue to secrete mineralized matrix. It is known that a relationship exists between ALP activity and mineralization, in which increased ALP activity propagates inorganic phosphate production until the onset of mineralization. Upon mineralization, ALP activity decreases, as it is no longer needed as the mineralized matrix matures. In our results, ALP activity was still increasing at day 21. This indicates that further mineralization could be detected if we were to continue to run the in vitro study beyond day 21. This observation is important because, as indicated on the compressive modulus vs. calcium concentration graph (Fig. 7A) the mechanical rigidity of the injectable orthobiologic material would continue to increase with cultivation time.

Mineralization within the PN-COL +osteo samples was also confirmed using histological analysis, SEM micrographs, and EDS spectrum data. The von Kossa staining conducted on histological slices revealed the progression of cell proliferation and mineralized matrix secretion within the PN-COL +osteo injectable scaffold. The histological images of the PN-COL +osteo scaffold demonstrated significant mineralization over time (day 7 to day 21) as indicated by the dark brown von Kossa staining (Fig. 5C and D). At day 21, SEM micrographs (Fig. 4A and B) show no sign of mineralization within the control PN-COL −osteo samples, while mineral crystals were observed within PN-COL +osteo samples. The EDS spectral analysis and elemental mapping agree with the ALP activity, alizarin red, and histology data. Fig. 4C–F shows elemental maps of calcium and phosphorus for the same area of PN-COL +osteo and control scaffolds on day 21. In the calcium mapping images (Fig. 4C and D), no calcium was revealed within the control scaffold (Fig. 4C) while calcium was abundant and was distributed throughout the PN-COL +osteo sample (Fig. 4D). In phosphate mapping images (Fig. 4E and F), the phosphate amount was higher within PN-COL +osteo material (Fig. 4F). However, as indicated by the EDS spectrum data, the same conclusion could not be drawn because the gold (Au) used to sputter coat the samples for SEM analysis shares the same energy level with phosphate. Thus, the peak observed around 2 keV in Fig. 4G and H might be a combined

effect of Au and phosphate. The EDS spectral analysis also confirmed the presence of calcium within PN-COL +*osteo*, whereas only trace amounts of calcium were detected for the PN-COL −*osteo* group (control group) (Fig. 4G and H).

The aforementioned biological results demonstrated that mineralization was present within the PN-COL +*osteo* scaffolds. Therefore, mechanical analyses were conducted to identify the relationship between *in situ* mineralization and the mechanical properties of the injectable orthobiologic scaffold. In order to characterize the temporal relationship between mechanical properties and *in situ* mineralized matrix formation, a confined compression stress-relaxation analysis was conducted and the collected data was fit to the standard linear solid mathematical model.

The PN-COL +*osteo* scaffolds demonstrated significant increases in compressive modulus, peak stress, and equilibrium stress in conjunction with significant increases in calcium deposition. At Day 0, the compressive modulus of PN-COL −*osteo* and PN-COL +*osteo* scaffolds were both around 1.5 kPa. For PN-COL −*osteo* scaffolds (control group), there were no changes in the compressive modulus after 21 days of cultivation. On the other hand, for the PN-COL +*osteo* group, the compressive modulus increased 3.3-fold over 21 days (Fig. 6D). The demonstrated increase in the compressive modulus can be attributed solely to the effect of *in situ* cellular-based mineralization on the compressive rigidity of the osteoconductive injectable material. Due to the logarithmic increment in the compressive modulus over time (Fig. 6D), we would expect to have a higher compressive modulus for the PN-COL +*osteo* group after day 21. The equilibrium and peak stress data (Fig. 7A and B) were consistent with the compressive modulus data and indicate that the compressive stress within PN-COL +*osteo* increased with *in situ* mineralization.

The standard linear solid (SLS) Model was presented to describe the changes in viscoelastic parameters because of *in situ* mineralization within the PN-COL +*osteo* scaffold. The results from the predictive mathematical model presented a good agreement with the experimental data over 21-day cultivation time for PN-COL +*osteo* scaffolds (Fig. 7B). The parameters describing the viscoelastic material properties of the PN-COL scaffolds (K_e, K_1, η, τ) (Table 1) also demonstrated apparent increases after 21 days of culture due to increased mineralized matrix formation. These results clearly indicated that the mechanical properties of the scaffold were enhanced solely due to increased *in situ* mineralization.

Synthetic mineralization, which can be defined by incorporation of organic minerals (hydroxyapatite, calcium phosphate and its derivatives) into the scaffold or onto the scaffold, has been used to enhance the mechanical properties of solid bone tissue scaffolds (Heinemann et al., 2011; Khanarian et al., 2012; Li et al., 2013). The literature cites several examples for increased mechanical properties due to synthetic mineralization. Heinaman et. al. utilize a chemically crosslinked collagen scaffold with incorporated hydroxyapatite (HA) and silica. Heinaman's group was able to demonstrate a similar fold increase (near 3-fold) in young's modulus from 0.4 MPa to 1.0 MPa. Kane and Roeder were able to demonstrate a near 8-fold increase in a freeze dried collagen scaffold from near 25 kPa (no HA reinforcement) to

near 200 kPa (with HA reinforcement). It is important to note that these scaffolds are solid state, non-injectable scaffolds. These features contribute to the apparent superior mechanical properties as compared to the PN-COL which sacrifices initial mechanical rigidity for physical properties which allow for its injectable nature.

Mineralization of the scaffold induced an increase in the compressive mechanical properties of the scaffold; however, the compressive modulus of the scaffold is still several orders of magnitude below that of cancellous bone reported between 0.01 and 100 GPa (Gibson, 1985). Therefore, the initial mechanical properties of the osteoconductive injectable scaffold are not sufficient for implantation into load bearing defects without external fixation. However, it is important to consider that not all bones are load-bearing tissue, for instance, craniofacial bones (except mandibular), calvarial, ulna, etc. Osteoconductive injectable scaffolds provide a potential clinical application in the treatment of non-load bearing bony defects.

In this study, we solely evaluated the effects of encapsulated cells and cellular processes on the mechanical properties of the injectable PN-COL scaffold. The results have demonstrated that cell-mediated mineralization increases the mechanical properties of the injectable PN-COL material. This study can initiate a new set of discussions on osteoconductive injectable materials as bone fillers and provide insight toward the development of mineralized bone tissue scaffolds.

5.   Conclusion

The present study incorporated pre-osteoblast cells within an injectable orthobiologic material in order to investigate the temporal relationship between *in situ* mineralized matrix formation and the mechanical properties of the scaffold. Two conclusions were made from this study. First, cell number was maintained within the PN-COL scaffold and differentiated cells were able to demonstrate typical osteoblastic function as indicated by the formation of mineralized matrix throughout the PN-COL scaffolds. Second, upon formation of mineralized matrix, the mechanical properties of the PN-COL scaffold demonstrated significant increases, namely peak and equilibrium stresses and the compressive modulus, as dictated by the stress-relaxation confined compression as well as elastic moduli and viscosity as dictated by the standard linear solid mathematical model. We have proved that *in situ* mineralization created by encapsulated cells increased the mechanical properties of the injectable orthobiologic PN-COL scaffold by several folds within three weeks. This correlation between *in situ* mineralization and the mechanical properties of this osteoconductive injectable material provides critical information that can be used in designing and controlling the mechanical properties of injectable bone tissue engineering scaffolds.

Acknowledgments

REFERENCES

Arabmotlagh, M., et al., 2012. Nanocrystalline hydroxyapatite facilitates bone apposition to polymethylmethacrylate: histological investigation using a sheep model. J. Orthop. Res. 30 (8), 1290–1295.

Baylan, N., et al., 2013. Polycaprolactone nanofiber interspersed collagen type-I scaffold for bone regeneration: a unique injectable osteogenic scaffold. Biomed. Mater. 8 (4), 045011.

Blattert, T.R., Jestaedt, L., Weckbach, A., 2009. Suitability of a calcium phosphate cement in osteoporotic vertebral body fracture augmentation a controlled, randomized, clinical trial of balloon kyphoplasty comparing calcium phosphate versus polymethylmethacrylate. Spine 34 (2), 108–114.

Chen, Y., et al., 2012. In vitro biocompatibility and osteoblast differentiation of an injectable chitosan/nano-hydroxyapatite/ collagen scaffold. J. Nanomater.

Currey, J.D., 1969. Mechanical consequences of variation in mineral content of bone. J. Biomech. 2 (1), 1–11.

Currey, J.D., 1975. Effects of strain rate, reconstruction and mineral content on some mechanical-properties of bovine bone. J. Biomech. 8 (1), 81.

Currey, J.D., 1988. The effect of porosity and mineral-content on the youngs modulus of elasticity of compact-bone. J. Biomech. 21 (2), 131–139.

Currey, J.D., et al., 2001. Mechanical properties of nacre and highly mineralized bone. Proc. R. Soc. London, Ser. B 268 (1462), 107–111.

Deng, M., et al., 2011. Biomimetic structures: biological implications of dipeptide-substituted polyphosphazene-polyester blend nanofiber matrices for load-bearing bone regeneration. Adv. Funct. Mater. 21 (14), 2641–2651.

Ding, K., et al., 2013. A promising injectable scaffold: the biocompatibility and effect on osteogenic differentiation of mesenchymal stem cells. Biotechnol. Bioprocess Eng. 18 (1), 155–163.

Galovich, L.A., et al., 2011. Biomechanical, histological and histomorphometric analyses of calcium phosphate cement compared to PMMA for vertebral augmentation in a validated animal model. Eur. Spine J. 20, 376–382.

Gibson, L.J., 1985. The mechanical-behavior of cancellous bone. J. Biomech. 18 (5), 317–328.

Grafe, I.A., et al., 2008. Calcium-phosphate and polymethylmethacrylate cement in long-term outcome after kyphoplasty of painful osteoporotic vertebral fractures. Spine 33 (11), 1284–1290.

Heinemann, S., et al., 2011. Effect of silica and hydroxyapatite mineralization on the mechanical properties and the biocompatibility of nanocomposite collagen scaffolds. ACS Appl. Mater. Interfaces 3 (11), 4323–4331.

Heo, D.H., et al., 2009. Morphological changes of injected calcium phosphate cement in osteoporotic compressed vertebral bodies. Osteoporos. Int. 20 (12), 2063–2070.

Huang, Z., et al., 2009. A bone-like nano-hydroxyapatite/collagen loaded injectable scaffold. Biomed. Mater. 4 (5).

Huang, Z., et al., 2011. Biomimetic properties of an injectable chitosan/nano-hydroxyapatite/collagen composite. Mater. Sci. Eng., C 31 (3), 683–687.

Khanarian, N.T., et al., 2012. A hydrogel-mineral composite scaffold for osteochondral interface tissue engineering. Tissue Eng. Part A 18 (5-6), 533–545.

Li, Z.Y., et al., 2013. A tough hydrogel-hydroxyapatite bone-like composite fabricated in situ by the electrophoresis approach. J. Mater. Chem. B 1 (12), 1755–1764.

Liao, H.T., Chen, C.T., Chen, J.P., 2011. Osteogenic differentiation and ectopic bone formation of canine bone marrow-derived mesenchymal stem cells in injectable thermo-responsive polymer hydrogel. Tissue Eng. Part C 17 (11), 1139–1149.

Marelli, B., et al., 2011. Accelerated mineralization of dense collagen-nano bioactive glass hybrid gels increases scaffold stiffness and regulates osteoblastic function. Biomaterials 32 (34), 8915–8926.

Meng, Y., et al., Longitudinal evaluation of the mechanical properties of biomineralized osteoblasts. 2007 In: IEEE 33rd Annual Northeast Bioengineering Conference, 2007: 15-16.

Niranjan, R., et al., 2013. A novel injectable temperature-sensitive zinc doped chitosan/beta-glycerophosphate hydrogel for bone tissue engineering. Int. J. Biol. Macromol. 54, 24–29.

Roy, M.E., et al., 2001. Correlations between osteocalcin content, degree of mineralization, and mechanical properties of C-Carpio rib bone. J. Biomed. Mater. Res. 54 (4), 547–553.

Shazly, T.M., et al., 2008. Viscoelastic adhesive mechanics of aldehyde-mediated soft tissue sealants. Biomaterials 29 (35), 4584–4591.

Shen, H., et al., 2010. An injectable scaffold: rhBMP-2-loaded poly (lactide-co-glycolide)/hydroxyapatite composite microspheres. Acta Biomater. 6 (2), 455–465.

Shen, S.Q., et al., 2013. The design and features of apatite-coated chitosan microspheres as injectable scaffold for bone tissue engineering. Biomed. Mater. 8, 2.

Tarsuslugil, S.M., et al., 2013. Development of calcium phosphate cement for the augmentation of traumatically fractured porcine specimens using vertebroplasty. J. Biomech. 46 (4), 711–715.

Trickey, W.R., Lee, G.M., Guilak, F., 2000. Viscoelastic properties of chondrocytes from normal and osteoarthritic human cartilage. J. Orthop. Res. 18 (6), 891–898.

Wahl, D.A., Czernuszka, J.T., 2006. Collagen-hydroxyapatite composites for hard tissue repair. Eur. Cells Mater. 11, 43–56.

Wang, X., Schoen, J.A., Rentschler, M.E., 2013. A quantitative comparison of soft tissue compressive viscoelastic model accuracy. J. Mech. Behav. Biomed. Mater. 20, 126–136.

Welch, R.D., et al., 2002. Subchondral defects in caprine femora augmented with in situ setting hydroxyapatite cement, polymethylmethacrylate, or autogenous bone graft: biomechanical and histomorphological analysis after two-years. J. Orthop. Res. 20 (3), 464–472.

Xia, Y., et al., 2012. Bone tissue engineering using bone marrow stromal cells and an injectable sodium alginate/gelatin scaffold. J. Biomed. Mater. Res. Part A 100A (4), 1044–1050.

Yang, X.Y., et al., 2010. Preparation and characterization of trace elements-multidoped injectable biomimetic materials for minimally invasive treatment of osteoporotic bone trauma. J. Biomed. Mater. Res. Part A 95A (4), 1170–1181.

Yildirim, E.D., et al., 2011. Enhanced cellular functions on polycaprolactone tissue scaffolds by O-2 plasma surface modification. Plasma Processes Polym. 8 (3), 256–267.